INT. J. NUM. METH. HEAT FLUID FLOW, VOL 2, 503–516 (1992)

UNSTEADY NATURAL CONVECTION IN OPEN-ENDED VERTICAL CONCENTRIC ANNULI

M. A. I. EL-SHAARAWI* AND M. A. AL-ATTAS

Department of Mechanical Engineering, King Fahd University of Petroleum & Minerals, Dhahran 31261, Saudi Arabia

ABSTRACT

A finite-difference scheme is developed for solving the boundary layer equations governing the unsteady laminar free convection flow in open ended vertical concentric annuli. The initial condition considered for the creation of the thermal transient corresponds to a step change in temperature at the inner annulus boundary while the outer wall is maintained adiabatic. Numerical results for a fluid of $Pr = 0.7$ in an annulus of radius ratio 0.5 are presented. The results show the developing velocity and pressure fields with respect to space and time. Also, the important relationship between the annulus height and the induced flow rate is presented for various values of the time parameter starting from quiescence to the final steady state.

KEY WORDS Transient natural convection Concentric annuli

NOMENCLATURE

a	local heat transfer coefficient based on area of heat transfer surface $[= q/(T_w - T_0)]$
$\bar{a}$	average heat transfer coefficient over the annulus height $[= \bar{h}/\pi D_w l(T_w - T_0) = \int_0^l a\,dz/l]$
b	annular gap width $(= r_2 - r_1)$
C_p	specific heat of fluid at constant pressure
D	equivalent (hydraulic) diameter of annulus $(= 2b)$
D_w	diameter of heat transfer boundary $(= 2r_1)$
f	volumetric flow rate $[= \int_{r_1}^{r_2} 2\pi r u\,dr = \pi(r_2^2 - r_1^2)u_0$
f_{ss}	steady state (independent of time) value of $f = \int_{r_1}^{r_2} 2\pi r u_{ss}\,dr = (r_2^2 - r_1^2)u_{oss}$
F	dimensionless volumetric flow rate $[= f/\pi l \nu Gr^* = (1 - N^2)U_0]$
F_{ss}	steady-state value of F $[= (1 - N^2)U_{oss}]$
F_{fd}	steady-state fully-developed value of F
g	gravitational body force per unit mass (acceleration)
Gr	Grashof number $[= g\beta(T_w - T_0)D^3/\nu^2]$
Gr^*	modified Grashof number $(= DGr/l)$
h	heat gained by fluid from the entrance up to a particular elevation in the annulus $[= \rho_0 f C_p(T_m - T_0)]$
$\bar{h}$	heat gained by fluid from the entrance up to the annulus exit, i.e., value of h at $z = l$ $[= \rho_0 f C_p(\bar{T}_m - T_0)]$

* On leave from Mechanical Engineering Department, Alazhar University, Nasr City, Cairo, Egypt.

0961–5539/92/060503–14$2.00

Received June 1992
Revised September 1992

H dimensionless heat absorbed from the entrance up to any particular elevation $= h/[\pi\rho_0 C_p lvGr^*(T_w - T_0)] = F\theta_m = 2\int_N^1 UR\theta\, dR$

$\bar{H}$ dimensionless heat absorbed from the entrance up to the annulus exit, i.e., value of H at $z = l$ $\{= \bar{h}/[\pi\rho_0 C_p lvGr^*(T_w - T_0)] = F\bar{\theta}_m = 2\int_N^1 UR\theta\, dR\}$

$\bar{H}_{fd}$ steady-state fully-developed value of H

K number of time increments needed to reach steady-state conditions

l height of annulus

L dimensionless height of annulus $(= 1/Gr^*)$

m number of axial steps in the numerical grid

n number of radial increments in the numerical grid

N annulus radius ratio $(= r_1/r_2)$

Nu local Nusselt number $(= aD/\kappa)$

$\overline{Nu}$ average Nusselt number based on the area of the heat transfer surface over the whole annulus height $(= \bar{a}D/\kappa)$

p pressure of fluid inside the channel at any cross-section

p' pressure defect at any point $(= p - p_s)$

p_0 pressure of fluid at the annulus entrance $(= -\rho_0 u_0^2/2)$

p_s hydrostatic pressure $(= -\rho_0 gz)$

P dimensionless pressure defect at any point $(= p' r_2^4/\rho_0 l^2 v^2 Gr^{*2})$

P_0 dimensionless pressure defect at annulus entrance $(= p_0 r_2^4/\rho_0 l^2 v^2 Gr^{*2} = -U_0^2/2)$

Pr Prandtl number $(= \mu C_p/\kappa)$

q heat flux at the heat transfer surface $[= -\kappa(\partial T/\partial r)_w]$

r radial coordinate

r_1 inner radius of annulus

r_2 outer radius of annulus

R dimensionless radial coordinate $(= r/r_2)$

Ra Rayleigh number $(= GrPr)$

Ra^* modified Rayleigh number $(= Gr^*Pr)$

t dimensionless time $(= \tau v/r_2^2)$

t_{ss} dimensionless steady-state time $(= \tau_{ss} v/r_2^2)$

T fluid temperature at any point

T_{ad} adiabatic wall temperature

T_m mixing cup temperature over any cross-section $= \int_{r_1}^{r_2} rut\, dr/\int_{r_1}^{r_2} ru\, dr$

$\bar{T}_m$ mixing cup temperature at exit cross-section, i.e., value of T_m at $z = l$

T_0 fluid temperature at annulus entrance

T_w temperature of the heat transfer boundary

u axial velocity component at any point

u_{ss} steady-state (independent of time) value of the axial velocity component at any point

u_0 entrance axial velocity $= \int_{r_1}^{r_2} 2\pi ru\, dr/[\pi(r_2^2 - r_1^2)]$

U dimensionless axial velocity component $(= ur_2^2/lvGr^*)$

U_0 dimensionless axial velocity at entrance $(= u_0 r_2^2/lvGr^*)$

U_{ofd} steady-state fully-developed of U_0

U_{oss} steady-state value of U_0 $(= u_{oss} r_2^2/lvGr^*)$

v radial velocity component at any point

V dimensionless radial velocity component (vr_2/v)

z axial coordinate

Z dimensionless axial coordinate $(= z/lGr^*)$

Greek symbols

β volumetric coefficient and thermal expansion
ν kinematic viscosity of fluid ($= \mu/\rho_0$)
μ dynamic viscosity of fluid
κ thermal conductivity of fluid
ρ fluid density at temperature T $\{= \rho_0[1 - \beta(T - T_0)]\}$
ρ_0 fluid density at inlet fluid temperature T_0
τ time
τ_{ss} steady-state time
θ dimensionless temperature at any point $[= (T - T_0)/(T_w - T_0)]$
θ_{ad} dimensionless adiabatic wall temperature at any height $[= (T_{ad} - T_0)/(T_w - T_0)]$
θ_m dimensionless mixing cup temperature at any cross-section $[= (T_m - T_0)/(T_w - T_0)]$
$\bar{\theta}_m$ dimensionless mixing cup temperature at exit cross-section, i.e., value of θ_m at $z = l$
θ_{fd} steady-state fully-developed value of θ
θ_{ss} steady-state value of θ

INTRODUCTION

In many practical engineering applications, the convective flow of most interest in a channel of any geometrical shape may consist mainly of transient or unsteady state. Also, unsteady natural convection heat transfer is of great importance in the design of control systems for modern free convection heat exchange devices. Moreover, processes which require the evaluation of the performance of thermal equipment in the unsteady free convection regime include start-up, shut-down, pump failure, etc. Despite the importance of the unsteady natural-convection heat transfer encountered in many engineering systems and applications, it has not received as much attention as its steady-state counterpart.

Because of its relative simplicity, the unsteady laminar free convection in the vicinity of a vertical flat plate has received almost exclusive attention of early analyses[1–9]. Transients in these analyses were created by a step change in wall temperature or wall heat flux. Nanda and Sharma[10] and Yang *et al.*[11] investigated the same case but with oscillatory surface temperature. Recently, Haq *et al.*[12] numerically investigated the case of transient free convection of a non-Newtonian fluid along a vertical flat plate. Analytical and experimental investigations related to transient free convection heat transfer on vertical surfaces and in vertical cylinders have been reviewed by Ede[13] and Hess and Miller[14], respectively.

Natural convection in confined fluids is of greater practical interest. For example, natural convection in a vertical channel formed by two parallel plates is encountered in many engineering applications including the cooling of electronic equipment and the heating of buildings via Trombe walls. Kettleborough[15] considered the transient laminar free convection between two suddenly heated vertical parallel plates at the same constant temperature. Lee *et al.*[16] investigated numerically and experimentally the unsteady natural convection heat and mass transfer in the parallel plate vertical channel but with asymmetric boundary conditions.

The present investigation is concerned with transient natural convection heat transfer in open-ended vertical concentric annuli. Important applications for such a problem may be found in double-pipe heat exchangers and in the transient natural convection which takes place around the fuel elements of a nuclear reactor during shut-off periods. A survey of the literature shows that transient natural convection in open-ended vertical annular passages has not yet been investigated analytically or experimentally. Only steady-state natural convection in vertical

annular passages has been considered in the literature[17–19]. The steady-state (with respect to time) solutions are of particular interest to the present investigation since a complete transient solution is obtained with the steady-state solution approached as the limiting solution for long times.

The lack of either theoretical or experimental data concerning unsteady natural convection in vertical concentric annuli, motivated the present investigation. In the present study, an iterative finite-difference scheme has been developed for solving the coupled conservation equations of mass, momentum, and energy which govern the transient laminar free convection flow in open-ended vertical annular passages. The developed finite-difference scheme and numerical method of solution can be considered as an indirect extension of the original work of Bodoia and Osterle[20] to include the case of transient free convection heat transfer. The initial condition, which creates the thermal transient, considered in the present investigation corresponds to a step change in the temperature of the inner wall of the annulus while its outer wall is kept adiabatic.

GOVERNING CONSERVATION EQUATIONS

Consider a vertical open-ended concentric annulus of a length l, open at both ends, immersed in a Newtonian fluid of infinite extent maintained at a constant temperature T_0. Initially, at time $\tau = 0$, the annulus inner and outer walls are in thermal equilibrium with the surrounding air inside and outside the annular passage (at same temperature T_0). At time $\tau > 0$, let the inner wall of the annulus be suddenly heated to a temperature greater than that of the surrounding fluid while the other wall is insulated. The fluid in the annular gap between the two cylindrical walls is suddenly set into motion by temperature-induced buoyancy forces. Fluid rises in the annular gap and is assumed to enter the channel at the ambient temperature T_0 with a uniform velocity u_0 which is changing with time. *Figures 1a–1c* depict the geometry, coordinate system, and the finite-difference grid used. The fluid has constant physical properties but obeys the

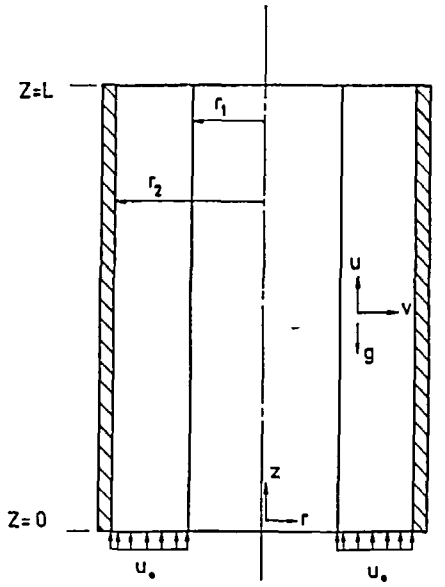

Figure 1a The geometry and coordinate system

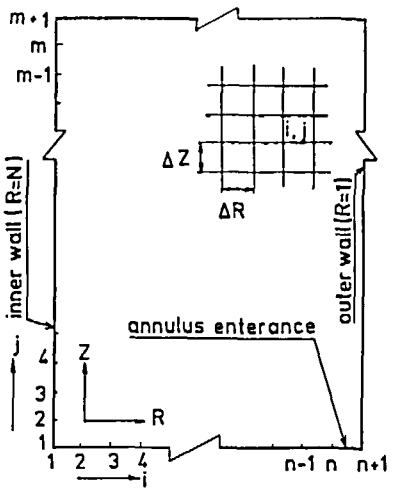

Figure 1b The numerical grid in R–Z plane

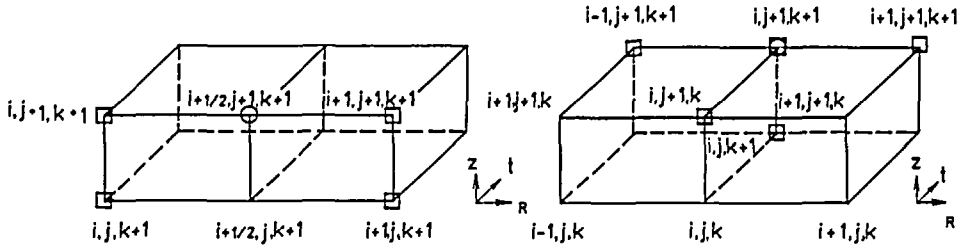

Figure 1c Three-dimensional grid showing points involved in the finite difference representations of the continuity, axial momentum, and energy equations

Boussinesq approximation, according to which its density is constant except in the buoyancy term of the vertical (axial) momentum equation. Axial symmetry and laminar flow conditions are assumed. Both viscous dissipation and axial conduction of heat are neglected. Further, applying the boundary-layer assumptions, which are valid when inertial forces are large relative to viscous forces, and using the dimensionless parameters given in the nomenclature, the motion and heat transfer are described by the solution of the following coupled dimensionless boundary layer equations.

$$\frac{\partial V}{\partial R}+\frac{V}{R}+\frac{\partial U}{\partial Z}=0 \tag{1}$$

$$\frac{\partial U}{\partial t}+V\frac{\partial U}{\partial R}+U\frac{\partial U}{\partial Z}=-\frac{\partial P}{\partial Z}+\frac{\theta}{16(1-N)^4}+\frac{1}{R}\frac{\partial}{\partial R}\left(R\frac{\partial U}{\partial R}\right) \tag{2}$$

$$\frac{\partial \theta}{\partial t}+V\frac{\partial \theta}{\partial R}+U\frac{\partial \theta}{\partial Z}=\frac{1}{Pr}\frac{1}{R}\frac{\partial}{\partial R}\left(R\frac{\partial \theta}{\partial R}\right) \tag{3}$$

These three coupled equations (1)–(3) are subject to the following initial conditions. For $t = 0$, $U = V = \theta = 0$ everywhere. On the other hand, for $t > 0$, the following boundary conditions are applicable:

$$\begin{aligned}
&Z = 0 \text{ and } N < R < 1: V = \theta = 0, U = U_0, \text{ and } P = P_0 = -U_0^2/2, \text{ where } U_0 \text{ is a function of time } t\\
&Z \geqslant 0 \text{ and } R = N: U = V = 0 \text{ and } \theta = 1\\
&Z \geqslant 0 \text{ and } R = 1: U = V = 0 \text{ and } \partial\theta/\partial R = 0\\
&Z = L, P = 0
\end{aligned} \tag{4}$$

It is noteworthy that the radial momentum equation has been dropped due to the boundary-layer assumptions. However, it is possible, under the linearized finite-difference scheme of Bodoia and Osterle[20], to compensate for the lack of such an equation by using the following dimensionless integral continuity equation

$$F = 2\int_N^1 RU\,dR = (1-N^2)U_0 \tag{5}$$

FINITE-DIFFERENCE EQUATIONS AND SOLUTION METHOD

Due to symmetry about the z-axis, only half of the channel has to be considered. A three-dimensional grid in R, Z and t has to be imposed on half of the annular passage. The

rectangular grid shown in *Figure 1b* is in the $R-Z$ plane and it may be used to depict the solution at a given time t. For each other value of time, say $t + \Delta t$, there is another grid exactly similar to that shown in *Figure 1b* but lies in a plane parallel to it. The non-dimensional time (t) is simulated by a third coordinate normal to the $R-Z$ plane as shown in *Figure 1c*. A typical mesh point is designated by three integer variables (i, j and k), with i progressing in the radial direction, $i = 1$ at the inner wall, $i = n + 1$ at the outer wall (n = number of radial increments in the mesh network), j progressing in the axial direction, $j = 1$ at the inlet cross-section, $j = m + 1$ at the exit cross-section ($Z = L$), m = number of axial increments in the mesh network ($m = L/\Delta Z$), k progressing in the hypothetical time direction, $k = 1$ at the initial state, and $k = K + 1$ at the final chosen value of time (K = number of time increments which is chosen such that steady-state conditions are achieved). The dependent variables are designated as point functions with subscripts (i, j, k).

By an indirect extention of the work of Bodoia and Osterle[20], (1)–(3) and (5) can be written in the following finite-difference forms, respectively:

$$\frac{V_{i+1,j+1,k+1} - V_{i,j+1,k+1}}{\Delta R} + \frac{V_{i+1,j+1,k+1} + V_{i,j+1,k+1}}{2[N + (i - \frac{1}{2})\Delta R]} + \frac{U_{i+1,j+1,k+1} + U_{i,j+1,k+1} - U_{i+1,j,k+1} - U_{i,j,k+1}}{2\Delta Z} = 0 \tag{6}$$

$$\frac{U_{i,j+1,k+1} - U_{i,j+1,k+1}}{\Delta t} + V_{i,j,k}\frac{U_{i+1,j+1,k+1} - U_{i-1,j+1,k+1}}{2\Delta R} + U_{i,j,k}\frac{U_{i,j+1,k+1} - U_{i,j,k+1}}{\Delta Z} = \frac{P_{j,k+1} - P_{j+1,k+1}}{\Delta Z} + \frac{U_{i+1,j+1,k+1} - 2U_{i,j+1,k+1} + U_{i-1,j+1,k+1}}{(\Delta R)^2} + \frac{1}{N + (i-1)\Delta R}\frac{U_{i+1,j+1,k+1} - U_{i-1,j+1,k+1}}{2\Delta R} + \frac{\theta_{i,j+1,k+1}}{16(1-N)^4} \tag{7}$$

$$\frac{\theta_{i,j+1,k+1} - \theta_{i,j+1,k}}{\Delta t} + U_{i,j,k}\frac{\theta_{i,j+1,k+1} - \theta_{i,j,k+1}}{\Delta Z} + V_{i,j,k}\frac{\theta_{i+1,j+1,k+1} - \theta_{i-1,j+1,k+1}}{2\Delta R} = \frac{1}{Pr}\left[\frac{\theta_{i+1,j+1,k+1} - 2\theta_{i,j+1,k+1} + \theta_{i-1,j+1,k+1}}{(\Delta R)^2} + \frac{1}{N + (i-1)\Delta R}\frac{\theta_{i+1,j+1,k+1} - \theta_{i-1,j+1,k+1}}{2\Delta R}\right] \tag{8}$$

$$F = 2\Delta R \sum_{i=2}^{n} U_{i,j,k+1}[N + (i-1)\Delta R] = (1 - N^2)U_0 \tag{9}$$

In the above implicit finite-difference equations (6)–(8), backward differences are used to replace the first derivatives with respect to time and axial distance ($\partial/\partial t$ and $\partial/\partial z$), central

differences are used to replace the first derivatives with respect to the radial coordinate ($\partial/\partial R$), and a conventional three-point difference is used to replace the second derivative with respect to $R(\partial^2/\partial R^2)$. In either (7) or (8), two levels of time are present and designated by k and $k+1$; the variables with subscript $k+1$ represent unknowns and those with subscript k are knowns. Similarly, for a given time (i.e., value of k) the variables with subscript $j+1$ represent unknowns and those with subscript j are knowns. Also, applying numerical stability theories[21] shows that the finite-difference equations (6)–(8) are consistent representations of the boundary-layer equations (1)–(3) and are stable for all mesh sizes as long as the downstream axial velocity is non-negative (i.e., there are no flow reversals within the domain of solution).

For a given fluid (i.e., a special value of Pr) in an annulus of given N and L, the numerical solution is obtained by first assuming a value of U_0. This is equivalent to either assuming the flow rate F or the inlet pressure P_0 since the former and the latter are linked to U_0 through (5) and (4), respectively. Then starting with $k=1$ (i.e., a time step Δt) and applying (8) with $j=1$ (annulus entrance cross-section) and $i=2,3,\ldots,n+1$ (taking into account that, according to the boundary conditions (4), $\theta_{n+2,j,k}=\theta_{n,j,k}$), we get n simultaneous linear algebraic equations which when solved (e.g., by Thomas' method[22]) give the values of the n unknown temperatures at all points of the second cross-section ($\theta_{2,2,2}, \theta_{3,2,2}, \ldots, \theta_{n,2,2}$ and $\theta_{n+1,2,2}$). Now, applying (7) with $i=2,3,\ldots,n$ and (9) to the entire cross-section we obtain n equations which when solved (e.g., by a special form of Gauss–Jordan elimination scheme[21]) give the values of the n unknowns ($U_{2,2,2}, U_{3,2,2}, U_{4,2,2}, \ldots, U_{n,2,2}$ and $P_{2,2}$) at all points of the second cross-section. Using the computed values of U's and applying (6) we get the values of V's at all points of the second cross-section. Keeping $k=1$ and repeating this procedure ($j=2,3,\ldots,m$), we advance section by section along the annulus until the final cross-section ($j=m+1$) is reached and its pressure value is obtained ($P_{m+1,2}$). If this obtained pressure value is zero (within an acceptable tolerance) the assumed value of U_0 is correct, otherwise a new value should be tried and the whole process is repeated. The acceptable tolerance in $P_{m+1,2}$ (pressure at exit cross-section) may be an arbitrarily chosen value below which the obtained numerical results become practically unaffected. In the present investigation the tolerance in $P_{m+1,k}$ is taken as $\pm 10^{-15}$.

Having obtained the accurate value of U_0 (for which $P_{m+1,2}=0$), this is the solution value of U_0 at $t=\Delta t$ and the corresponding obtained values of T's, U's, P's, and V's represent the required numerical solution of this particular time ($t=\Delta t$). Now, we can advance other steps in the time domain by repeating the aforesaid whole process with $k=2,3,4,\ldots$ until steady-state conditions (with respect to time) are achieved. Steady-state conditions mean that the obtained values of T's, U's, P's and V's would not change with further increase in the value of time (i.e., with further increase in the value of the counter k). Of course, this latter statement is applicable in a computer program with an arbitrarily chosen acceptable tolerance. In the present investigation, it was considered that steady-state conditions are reached when the variation in the value of the overall heat absorbed by the fluid inside the annulus ($\bar{H}$) does not exceed an absolute value of 0.001% with further increase in time [i.e., $(\bar{H}_{k+1}-\bar{H}_k)/\bar{H}_{k+1} \leqslant \pm 10^{-6}$].

In fact, there is nothing new in the chosen conventional finite-difference approximations in (6) to (9). However, the chosen finite-difference approximations are not of the same form in all the equations. This has been deliberately done so as to insure stability of the numerical solution and to enable the equations to be solved in the previously mentioned manner. Moreover, in practice, for a confined free convection flow, such as that given under consideration, the channel height is normally known (i.e., L is given) while the volumetric flow rate f (hence F) is unknown. The numerical method of solution for steady-state cases[17,18] differs from the present method of solution as follows. The steady-state method of solution[17,18] handles the problem in a reversed manner by obtaining an unknown channel height for a given volumetric flow rate. On the other

hand, the present numerical method of solution iteratively obtain the unknown transient flow rate (as a function of time) for a given annulus height.

It may be worth reporting examples of the grid sizes used in the present investigation. The axial and time increments, for both cases (I) and (O), were as follows. For $Gr^* = 10^5$: $\Delta Z = 2 \times 10^{-7}$ and $\Delta t = 10^{-3}$; for $Gr^* = 10^4$: $\Delta Z = 2 \times 10^{-6}$ and $\Delta t = 10^{-3}$, and for $Gr^* = 10^3$: $\Delta Z = 2 \times 10^{-5}$ and $\Delta t = 5 \times 10^{-3}$. The number of radial increments was 40 in all the computer runs.

RESULTS AND DISCUSSION

Computations were carried out for a fluid of $Pr = 0.7$ in an annulus of $N = 0.5$. The radius ratio 0.5 was chosen since it represents a typical annular geometry with its value of N far enough from unity ($N = 1$) which represents the case of a parallel plate channel. Moreover, steady-state developing solutions for this particular radius ratio are available in the literature[17]. Such steady-state solutions provide a mean to check the adequacy of the transient solutions to be obtained in the present investigation. The transient solutions should asymptotically approach these steady-state solutions.

It is important to mention that the present thermal boundary conditions give, in a sufficiently high annulus, a steady-state solution (at large values of t) which approaches (at large values of Z) the fully-developed solution of the third kind[19]. For this particular limiting case the analytical steady-state fully-developed solution is available[19] and accordingly the upper limiting values of the steady-state dimensionless volumetric flow rate (F) and the dimensionless heat absorbed by the fluid over the entire channel height are equal and given in the annulus under consideration ($N = 0.5$), by:

$$F_{fd} = \bar{H}_{fd} = 0.015748 \tag{10}$$

From (10) the corresponding upper-limiting steady-state values of U_0 and P_0 (U_{ofd} and P_{ofd}) are 0.0209973 and $-2.2044414 \times 10^{-4}$, respectively.

Equation (10) merely states that it is impossible, in a purely laminar natural convection regime through a vertical annulus of $N = 0.5$ with an isothermal boundary, to have a dimensionless volumetric flow rate (F) greater than 0.015748, otherwise there must be an external force aiding the buoyancy driving force. In other words, the steady-state dimensionless volumetric flow rate (F) reaches an upper asymptotic value as the annulus height approaches infinity. This means that, in an annulus with an isothermal boundary, when the channel becomes sufficiently high so that the steady-state flow reaches its state of full development, a further increase in the channel height would not produce any further increase in the sucked steady volumetric flow rate. Such a special characteristic of free convection flows in channels with an isothermal boundary guides the choice of the values of U_0 (i.e., $U_0 < U_{oss} < U_{ofd}$ hence $F < F_{ss} < F_{fd}$). In the present investigation, values of the dimensionless channel height L (i.e., values of Gr^*) were selected to give a wide range of steady-state dimensionless flow rates (F_{ss}) which approaches its fully developed value F_{fd}. The investigated values of L range from 10^{-5} to 0.25; thus the investigated range of modified Grashof number (Gr^*) is $4 \leqslant Gr^* \leqslant 10^5$. On the other hand, the accuracy of the present computer code was tested by the excellent agreement which was achieved between the present steady-state solutions (obtained at considerably large values of time) and the existing numerical and analytical solutions reported by one of the authors in two previous papers[17,19].

Due to space limitations, only a representative sample of the results will be presented here. For the understanding of the physics of the problem under consideration, these results will include the developing transient axial velocity, radial velocity, and temperature profiles. On the

other hand, the results also include the time variations, along the channel, of the pressure distribution, the adiabatic wall temperature, the mixing cup temperature or the heat absorbed by the fluid, and the $F-L$ relationship since these are more important to thermal and control engineers than the temperature and velocity profiles. Also, the variation of the steady-state time (t_{ss}) with the channel height (L) will be given.

Figure 2 gives the developing axial velocity profiles with time at mid-channel height for a value of $Gr^* = 4$ ($L = 0.25$). So, this Figure is for a very small value of Gr^* which means a long annulus with a small hydraulic diameter and a low temperature difference. Therefore, it is expected, in such a case, that the velocity profile will approach the fully developed profile at the annulus exit. Comparing the velocity profile corresponding to the largest value of time (t) in this Figure with the available fully developed solution of the third kind[19], it can be seen that the flow has almost reached its stage of full development, even though it is still at mid-channel height. This means that for larger values of Z and/or t the axial velocity profile remains almost unchangeable. On the other hand, this comparison provided an excellent check on the adequacy of the present numerical results.

Another interesting observation from *Figure 2* is that at early times the axial velocity profiles have their peaks very close to the heated boundary. As the time increases the peak moves from the heated boundary towards the adiabatic boundary and approaches asymptotically its fully-developed radial location. This behaviour of the axial velocity profiles is indeed a consequence of the thermal boundary layer developing, with respect to both time and space, on the heated boundary. As the time increases the thermal boundary layer penetrates further into the fluid far from the heated wall. Thus, for a given axial position, as the time increases the buoyancy driving force is created in new regions far from the heated boundary and its value increases in old regions in which it was previously present. Therefore, the value of the axial velocity increases and its peak moves towards the unheated boundary as the time increases.

Figure 3 gives the mid-height temperature profiles corresponding to $Gr^* = 4$ for various selected values of the dimensionless time t. This Figure clarifies how the heat penetrates, as the time passes, into fluid regions far from the isothermal heated boundary. Moreover, at the largest time value presented in either Figure the temperature of the fluid all over the annular gab has become equal to the heated wall temperature. Thus the fluid at this particular time and location has reached its steady (with respect to time) fully developed (with respect to axial distance) state. This clarifies why the axial velocity profiles, shown in *Figure 2*, become at large times, identical to the steady-state fully-developed profiles given in Reference 19.

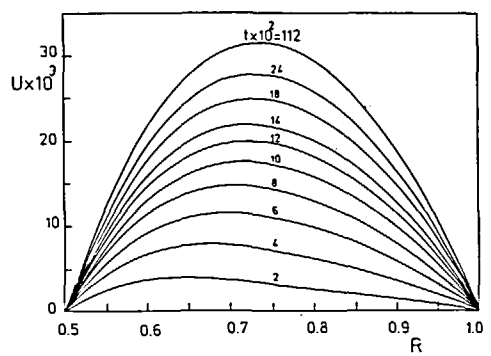

Figure 2 Mid-height U *versus* R for different values of t, $Gr^* = 4$

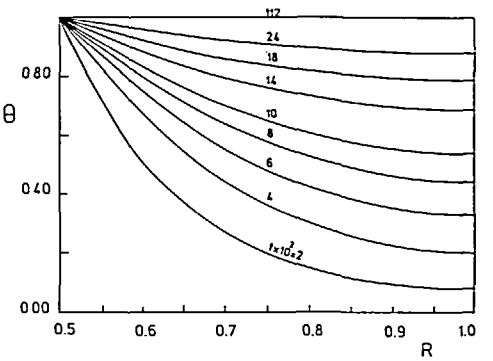

Figure 3 Mid-height θ *versus* R for different values of t, $Gr^* = 4$

Decreasing the annulus height to $L = 0.01$ (i.e., increasing the value of Gr^* to 100), unpresented results show the same previously mentioned characteristics of U and θ profiles. However, the flow reaches the annulus top exit without being fully developed ($\theta < 1$ and $U \neq U_{fd}$) at steady-state (sufficiently large values of t). To clarify this point, *Figure 4* gives examples of the mid-height radial velocity profiles at various selected values of the time t. Positive values of V mean that V is in the radial direction (from the inner wall to the outer wall) and *vice versa.* When the steady-state flow reaches full development V must equal zero everywhere in the annular gab. As can be seen from this Figure, at the largest value of time presented in the Figure, the radial velocity component has not decayed to its full development zero value. *Figure 4* also shows that, for the given axial location (mid-height), the radial velocity always transports fluid from regions close to the heated boundary towards the opposite adiabatic boundary and that its value increases as the time passes. This, together with the principle of continuity, clarify the previously mentioned behaviour concerning the motion of the peaks of the U profiles from regions near to the heated boundary towards the adiabatic boundary as the time elapses.

Now, decreasing the annulus height to $L = 0.001$ (i.e., increasing $Gr^*$to 1000) we obtain the same behaviour of the unsteady state U profiles but the steady-state profile deviates more from the fully developed profile. This is because the steady state temperature profiles do not reach the full development value ($\theta_{fd} = 1$) as clarified by the profiles corresponding to the largest value of t in *Figure 5a.* With larger values of Gr^*, the phenomenon of temperature overshoot starts to appear as may be observed from *Figure 5b.* In this Figure, the temperature profiles

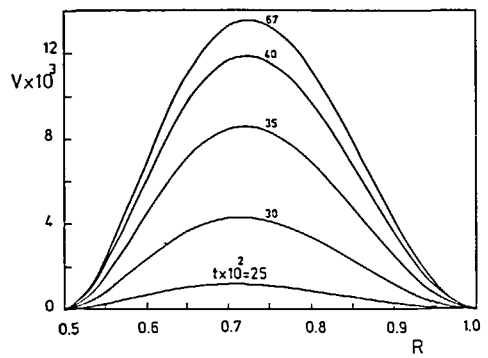

Figure 4 Mid-height V *versus* R for different values of t, $Gr^* = 100$

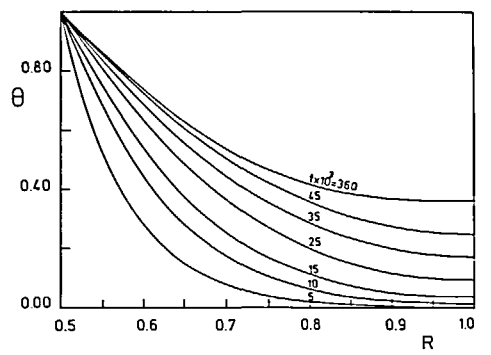

Figure 5a Mid-height θ *versus* R for different values of t, $Gr^* = 1000$

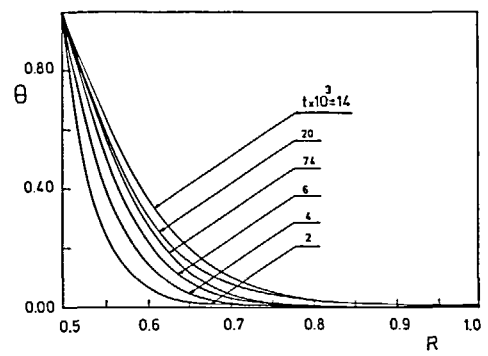

Figure 5b Mid-height θ *versus* R for different values of t, $Gr^* = 10^5$

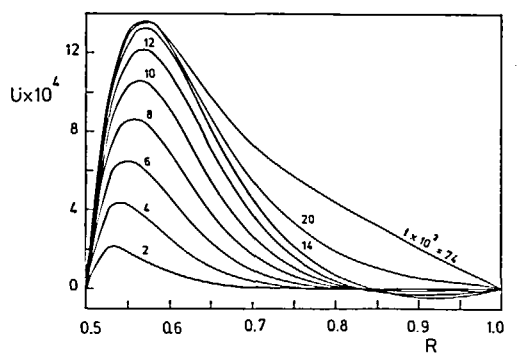

Figure 6 Mid-height U *versus* R for different values of t, $Gr^* = 10^5$

corresponding to $t = 14 \times 10^{-3}$ and $t = 2 \times 10^{-2}$ overshoot the steady-state temperature profile at $t = 74 \times 10^{-3}$. Such a phenomenon is known in transient heat transfer regimes[6]. Other unpresented results and also *Figure 5b* shows that this phenomenon becomes more pronounced as the value of Gr^* further increases (i.e., L further decreases, thus having a small value of dimensionless flow rate in a short annulus with a large hydraulic diameter and a large temperature difference). The profiles shown in *Figure 5b* also indicate that, at large values of Gr^*, the temperature step signal is felt only in regions close to the heat transfer surface. This type of temperature distribution is akin to that about a single vertical plate or cylinder in free convection.

It is worth mentioning that at sufficiently large values of Gr^* there exists a probability of flow reversals near the adiabatic wall. This prediction can be physically attributed to the fact that, when Gr^* becomes sufficiently large, the fluid accelerates near the heated boundary and, due to the continuity principle, it decelerates near the opposite insulated wall. Before the occurrence of a flow reversal, the axial velocity gradient normal to the adiabatic wall vanishes ($\partial u/\partial R|_{\text{wall}} = 0$). With a reversed flow, the slope of the axial velocity profile at the adiabatic wall becomes negative, values of U near this wall become also negative, the boundary layer flow model is unsuitable, and the numerical stability of the present finite-difference scheme becomes uncertain. This prediction has been confirmed at $Gr^* = 10^5$ as shown in *Figure 6*. In this Figure the axial velocity profiles have negative values near the adiabatic wall. However, at large values of time (t) the profiles could recover at this particular height. It is important to point out that, for a given time, if a flow reversal occurs at a given axial location it is anticipated that it continues downstream (at locations of larger heights). The present numerical scheme was able to continue the solution in some cases with flow reversals, as those shown in *Figure 6*, even though the condition for numerical stability ($U \geqslant 0$, i.e., non-negative U) is not satisfied in such cases. However, with values of Gr^* larger than this given in *Figure 6*, numerical instability occurred and solutions could not be obtained. Thus, even though numerical stability theories when applied to the present finite-difference scheme necessitate positive values for the axial velocity allover the domain of solution (i.e., no flow reversal), the computer program succeeded in obtaining numerical solutions for some cases where the reversed flow is small, as shown in *Figures 5b* and *6* for $Gr^* = 10^5$. However, one should bear in mind that the present boundary-layer model is not suitable for describing cases with flow reversals as large normal (radial) velocities exist near the flow reversal region and hence the accuracy of the boundary-layer approximations becomes questionable in this particular region.

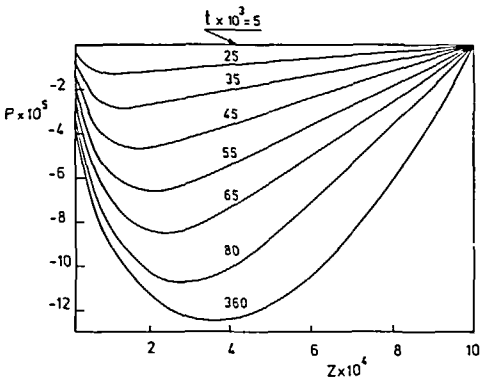

Figure 7 *P versus Z* for different values of t, $Gr^* = 1000$

Examples of the time-variations of the dimensionless pressure defect P along the channel are shown in *Figure 7*. Each curve corresponding to a given value of time is a typical pressure distribution in confined free convection channel flows. For a given time, the dimensionless pressure defect starts, at the annulus entrance, with a value which, according to Bernoulli's equation, equals to $-U_0^2/2$. Then the pressure decreases with Z until a minimum value is attained. In the region from the entrance until the cross-section at which P reaches its minimum value the fluid friction is larger than the buoyancy driving force and therefore the pressure decreases. However, as Z increases the buoyancy driving force develops and becomes larger than the fluid friction and the pressure defect therefore increases until it equals zero at the exit cross-section. As the time elapses, similar pressure defect distributions along the channel are obtained, but with lower values of pressure as a consequence of the increase in velocity values with time.

As stated before, thermal and control engineers are more interested in the mixing cup temperature and the adiabatic wall temperature. The practical importance of θ_m derives from the fact that it can be easily used to determine the heat gained by the fluid (H) without need of computing the temperature gradient at the heated boundary to get the local heat transfer coefficient (a) (from which Nu can be obtained), and then integrating to obtain the average heat transfer coefficient, $\bar{a}$ (from which $\overline{Nu}$ can be obtained). Samples of the variation of θ_m with respect to time and axial distance (from entrance) are shown in *Figure 8* while samples of the corresponding variation of the adiabatic wall temperature are given in *Figure 9*. As can be

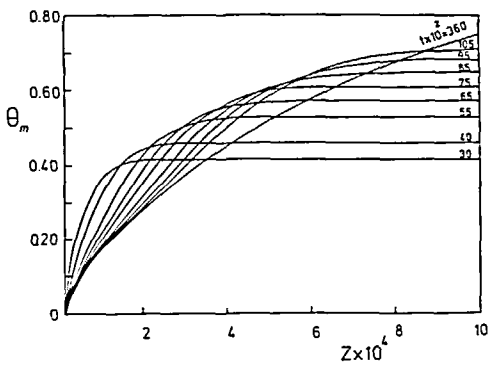

Figure 8 θ_m *versus* Z for different values of t, $Gr^* = 1000$

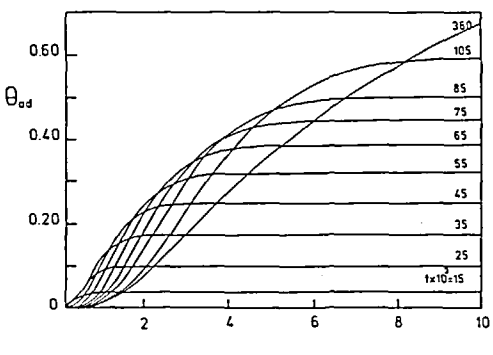

Figure 9 θ_{ad} *versus* Z for different values of t, $Gr^* = 1000$

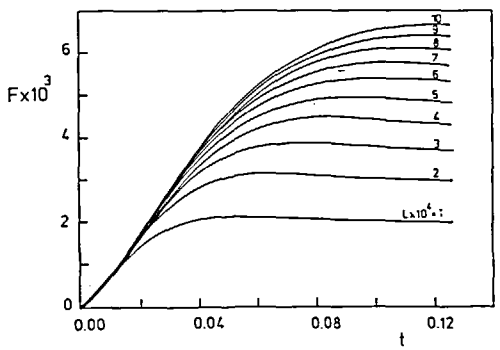

Figure 10 Variation of F with t for small values of L

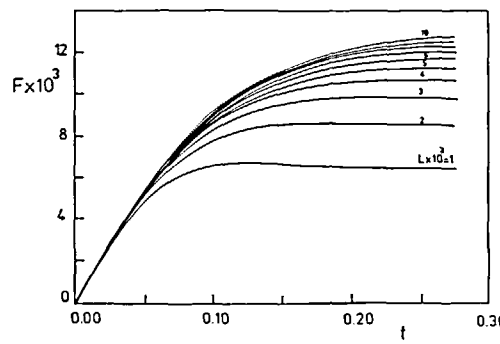

Figure 11 Variation of F with t for large values of L

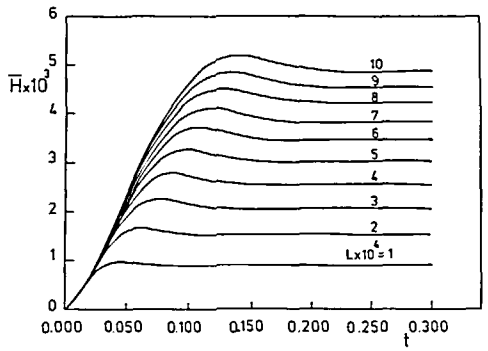

Figure 12 Vatiation of H with t for some selected values of L

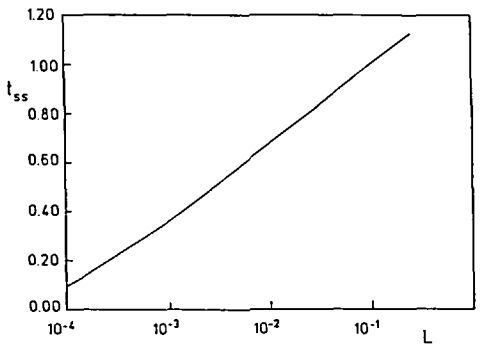

Figure 13 Variation of t_{ss} with L

seen from these Figures, at early times and near to the entrance θ_m and θ_{ad} decrease with time; this is attributed to the temperature overshoot phenomenon which has been mentioned before. However, as the time increases the behaviours of θ_m and θ_{ad} return to normal, i.e., they increase as the time increases. The early behaviour of θ_m means that the heat transfer coefficient drops, at early times (conduction time) and near the entrance, to values lower than its steady-state values then it recovers and increases to its steady-state value. Again such a phenomenon is known in the transient free convection literature[6].

It is very important, in engineering and control applications, to know the time variation of the sucked volumetric flow rate in a given annulus and also the time required to reach the steady-state conditions. *Figures 10* and *11* give the variation of F for small and large values of L, respectively. These curves together with the corresponding curves for θ_m can be used to obtain the time variation of H (since $H = F\theta_m$) for different annuli heights. *Figure 12* presents a sample of such results while *Figure 13* gives the steady-state time (t_{ss}) *versus* L. Finally, it is worth mentioning that a second check on the adequacy of the present numerical results was done by comparing the obtained steady results with those available in the literature[17] and excellent agreement was always found.

CONCLUSIONS

A finite-difference scheme has been developed to solve the boundary-layer equations governing the unsteady developing free convection in vertical open-ended concentric annuli. Obtained numerical solutions clarified the mechanism of development of both velocity and temperature fields with respect to time and space. The initial condition for creating the transient which has been considered corresponds to a step change in the inner wall temperature while the opposite wall is kept adiabatic. Reversed flows were observed at considerably large values of Gr^*.

REFERENCES

1 Siegel, R. Transient free convection from a vertical flat plate, *Trans. ASME*, **80**, 347–359 (1958)
2 Sparrow, E. M. and Gregg, J. L. Nearly quasi-steady free convection heat transfer in gases, *J. Heat Transfer*, **82**, 258–260 (1960)
3 Chung, P. M. and Anderson, A. D. Unsteady laminar free convection, *J. Heat Transfer*, **83**, 473–478 (1961)
4 Gebhart, B. Transient natural convection from vertical elements, *J. Heat Transfer*, **83**, 61–70 (1961)
5 Hellums, J. D. and Churchill, S. W. Computation of natural convection by finite-difference methods, *Proc. Int. Heat Transfer Conf.*, Part V, pp. 985–994 (1961)

6 Hellums, J. D. and Churchill, S. W. Transient and steady state, free and natural convection, numerical solutions: Part I. The isothermal, vertical plate. Part II. The region inside a horizontal cylinder, *AIChE J.*, **8**, 690–695 (1962)
7 Schetz, J. A. and Eichhorn, R. Unsteady natural convection in the vicinity of a doubly infinite vertical plate, *J. Heat Transfer*, **84**, 334–338 (1962)
8 Menold, E. R. and Yang, K. Asymptotic solutions for unsteady laminar free convection on a vertical plate, *J. Appl. Mech.*, **84**, 124–126 (1962)
9 Nanbu, K. Limit of pure conduction for unsteady free convection on a vertical plate, *Int. J. Heat Mass Transfer*, **14**, 1531–1534 (1971)
10 Nanda, R. S. and Sharma, V. R. Free convection laminar boundary layers in oscillatory flow, *AIAA J.*, **1**, 937–938 (1963)
11 Yang, J. W., Scaccia, C. and Goodman, J. Laminar natural convection about vertical plates with oscillatory surface temperature, *J. Heat Transfer*, **96**, 9–14 (1974)
12 Haq, S., Kleinstreuer, C. and Mulligan, J. C. Transient free convection of a non-Newtonian fluid along a vertical wall, *J. Heat Transfer*, **110**, 604–607 (1988)
13 Ede, A. J. Advances in free convection, in *Advances in Heat Transfer*, (Ed. T. F. Irvine and J. P. Hartnett), Vol. 4, Academic Press, New York, pp. 1–64 (1968)
14 Hess, C. F. and Miller, C. W. Natural convection in a vertical cylinder subject to a constant heat flux, *Int. J. Heat. Mass Transfer*, **22**, 421–420 (1979)
15 Kettleborough, C. F. Transient laminar free convection between heated vertical plates including entrance effects, *Int. J. Heat Mass Transfer*, **15**, 883–896 (1972)
16 Lee, T. S., Parikh, P. G., Acrivos, A. and Bershader, D. Natural convection in a vertical channel with opposing buoyancy forces, *Int. J. Heat Mass Transfer*, **24**, 499–511 (1982)
17 El-Shaarawi, M. A. I. and Sarhan, A. Developing laminar free convection in a heated vertical open-ended concentric annulus, *Ind. Eng. Chem. Fundam.*, **20**, 388–394 (1981)
18 Al-Arabi, M., El-Shaarawi, M. A. I. and Khamis, M. Natural convection in uniformly heated vertical annuli, *Int. J. Heat. Mass Transfer*, **30**, 1381–1389 (1987)
19 El-Shaarawi, M. A. I. and Al-Nimr, M. A. Fully developed laminar natural convection in open-ended vertical concentric annuli, *Int. J. Heat Mass Transfer*, **33**, 1873–1884 (1990)
20 Boidoia, J. R. and Osterle, J. F. The development of free convection between heated vertical plates, *J. Heat Transfer*, **84**, 40–44 (1962)
21 Carnahan, B., Luther, H. A. and Wilkes, J. O. *Applied Numerical Methods*, pp. 449–475, John Wiley, Chichester (1969)
22 Lapidus, L. *Digital Computation for Chemical Engineers*, McGraw-Hill, New York, pp. 254–255 (1962)